Software application for image based solid oxide fuel cell electrode microstructure characterisation

Periasamy Vijay,
DV IndAn
Email: periasamyvijay@dv-indan.com
Linkedin:https://www.linkedin.com/company/dv-indan
Github: https://github.com/Devetree/SOFC-IMG
URL: www.dv-indan.com

Abstract
Extracting microstructural parameters and properties of Solid Oxide Fuel Cell (SOFC) anode from microstructural images is essential for its characterisation. Obtaining good quality images and their efficient segmentation are crucial steps in ensuring the accuracy of the derived properties. To counter the drawbacks of the popularly used methods for image segmentation, I propose a compound algorithm (CA) consisting of thresholding and morphological operations. With only a few adjustable parameters, the algorithm reduces the volume fraction error to achieve better segmentation that can be verified by visual means. Microstructural properties and parameters including the contact angles between the phases are derived from the 2D images. A Matlab based application is developed based on the proposed algorithms for facilitating SOFC image analysis. This article describes the theory, methods and procedures used in the software application for deriving the microstructural properties of SOFC anode.
Keywords: SOFC anode; Microstructure characterisation; Image analysis; Segmentation

1. Introduction

Solid oxide fuel cells (SOFCs) are attractive energy conversion devices due to their versatility and high energy conversion efficiency. The reliability and performance degradation of SOFCs are affected by the microstructural properties of its electrodes. The microstructural properties of the electrodes including the electrochemical active area and the surface area of the constituent phases are controlled by the structural parameters such as volume fractions and particle sizes. This article focusses on the Ni–YSZ (Nickel –Yttria Stabilised Zirconia) anode, which is the most commonly used anode for SOFCs. Characterisation of the SOFC anode microstructure involves quantification of the properties from the microscopic images of the electrode.

Image analysis is the only method through which the microstructural properties can be measured and therefore it is important for optimising and tailoring the microstructure to obtain best performance. However, extracting the properties from the images is not straightforward as it involves many image processing and segmentation steps with high probabilities of introducing error. In addition, obtaining a good image with sufficient contrast between the phases has its challenges due to the many variables affecting the polishing and the imaging steps.

Many imaging techniques like optical microscopic imaging [1] [1, 2], secondary electron microscopic imaging (SEI) [3-5], Back Scattered Electron (BSE) imaging [6, 7] (sometimes with SEI) [3] have been used to characterise electrode microstructures. The technique used for microscopic imaging depend upon the material properties and the desired microstructural properties. Image resolution and image size needs to be suitable optimised for obtaining desired particles counts and contrast between the phases. In addition, the imaging conditions such as working distance, operating voltage and current etc., need to be optimised to get good quality images. Optical microscopy imaging techniques were used in Simwonis et al. [1], Lee et al. 2002, 2005 [2, 3] to characterise electrode microstructure. Nickel particles are distinguished in Ni-YSZ anode using optical microscopy due to high Back Scattered Coefficient of nickel but it is difficult to differentiate between YSZ and pore due to insufficient difference in grey intensity.

Optical imaging techniques require the sputtering of interference film during sample preparation process to decrease the contrast of nickel and to differentiate nickel, YSZ and pore phases in the anode. However, it is very tedious to control and optimise the thickness of interference film. Lee et

al. [3] have utilised Scanning Electron Microscopy (SEM) and optical microscopy to distinguish all three phases in anode. The Nickel phase is separated using optical microscopy and pores are separated using SEM imaging. Finally, Nickel is etched out from the sample using HCl (Hydrochloric Acid) to obtain the YSZ phase information. Thus, all the three phases are obtained in different images. Low voltage-SEM technique was used by Thyden et al. [4] to separate the anode constituent phases. For the low acceleration voltage, the phase contrast was found to decrease with increasing acceleration voltage. The back scattered coefficient is found to be dependent on acceleration voltage in the range of 1 to 5 KV. The lateral SE (Secondary Electron) detector is used to get the contrast between Ni and YSZ, with an acceleration voltage of 1 KV and a working distance of 10 mm. Faes et al.[5] also acquired the images with similar operating parameters for the imaging as used by Thyden et al. [4].

Monachon et al. [6] and Lanzini et al. [7] have used the high voltage BSE-SEM (Back Scattered Electron-Scanning Electron Microscopy) (around 20 kV) to get the contrast in anode constituents (Ni, YSZ and pore). This technique poses the challenge of resolution due to higher interaction volume of electron beam with the material. The above methodologies have been also used for microstructural investigation of electrodes including the effect of microstructural parameters on properties and the change in properties after cell operation [1] [3] [5]. These discussions illustrate that obtaining a good microstructural image that is suitable for segmentation of the phases is challenging.

Even if a decent image quality is obtained, the image processing and segmentation steps introduce additional uncertainties into the property derivation. While the thresholding method is predominantly used for the segmentation in SOFC electrodes [2] [7] [8] [9] [10] [11] [12] [13] [14], its limitations are also fairly recognised [15]. Although there are a few other methods suggested for electrode image segmentation [15] [13], a method that can work for all images is elusive [15]. This article presents a compound algorithm for the image segmentation that utilises the basic thresholding and morphological operations for image processing and segmentation. Algorithms are also presented for deriving the microstructural properties and parameters the 2D images. Specifically, the contact angles are derived from the 2D image for the first time. All these algorithms have been combined to create a graphical user interface in Matlab for facilitating SOFC image analysis. These contributions offer improvements to the image processing and segmentation methods for extracting accurate properties.

2. Image segmentation

Image segmentation is the process of segmenting images into meaningful parts based on the similarity of features or properties. Segmentation of the SOFC anode microstructural images into the three constituent phases, namely, Ni, YSZ and pore, is essential in order to derive the microstructural properties. Image segmentation methods are based on discontinuity detection or similarity detection of pixels in a region. Among the popular methods for segmentation that includes threshold method, edge based method, clustering based method, region based method, watershed based method [16], and Partial Differential Equation (PDE) based methods [17], optimizsation based methods [18],thresholding is the most widely used for segmenting SOFC electrodes[2] [7] [8] [9] [10] [11] [12] [13] [14] because of its simplicity and general effectiveness.

As mentioned in [15], a general segmentation method that works for all possible microstructures does not exist. This may be due to the presence of several factors that can influence the quality of the image in different ways. While general thresholding using Otsu’s method did not produce acceptable results for our images, other methods involve complexities, which may require specialised treatment of individual images. For example, [15] proposed a region growing method for segmentation where pixels of known phases are chosen as seeds and the algorithm grows the regions according to some rules until the edges are reached. However, it is found in our case that edges have discontinuities due to the poor image quality. Therefore, a region-growing algorithm will not be successful for these images. An algorithm that uses basic thresholding and

morphological operations could be much suitable for improving the image processing and segmentation accuracy.

The algorithm presented in this article is motivated by and attempts to exploit the following observations. The pore phase in the images is generally well defined and distinguishable as discussed. The difficulty in segmentation is higher in the allocation of pixels between the Ni and the YSZ phases due to less contrast between them. Conventional thresholding methods like Otsu's method result in underestimating the Ni phase pixels forming thin strips of YSZ phase around the Ni phase. This observation was also reported in [15]. Theoretical volume fractions of the phases in the electrode can be calculated and are often used to ascertain the accuracy of the segmentation process [5-8, 13-15, 19-23]. The volume fraction errors of the phases can be used to guide the segmentation process.

This article proposes an algorithm to exploit the above observations, which consists of the following steps.

1 Otsu's thresholding
2 Automatic threshold adjustment
3 Sweep fill operation
4 Erosion and dilation

The first step is performing the Otsu's thresholding on the grey scale image. This results in two thresholds, namely T_1 and T_2. The pore is the darkest phase, while Ni is the lightest with YSZ having an intermediate intensity. A grey scale image consist of intensities between 0 to 255 with 0 being the darkest (black) and 255 the lightest (white). Therefore, the threshold T_1 represents the intensity at the boundary between the pore and the YSZ phases, while T_2 forms the boundary between the YSZ and the Ni phases.

The aim of the second step is to minimise the error in the volume fractions resulting from thresholding and the theoretically calculated ones. However, only the threshold T_1 is manipulated as the pore phase is well defined generally. Adjustment of threshold T_2 results in improper spatial allocation of pixels between Ni and YSZ. Therefore, the threshold adjustment step only minimises the error in the pore volume fraction by manipulating the threshold T_1.

The volume fractions of the phases are derived from the image using the most fundamental stereological relationship, Delesse-Rosiwal law given as, , $V_V = A_A$ where, V_V is the volume fraction of a phase of interest in the 3D volume and A_A is the area fraction of a phase of interest divided by the total area of the specimen image. The volume fraction of a particular phase in the image is the ratio of the number of pixels representing that phase to the total number of pixels in the image.

The algorithm for the threshold adjustment is as the following.

1 Calculate pore volume fraction of the image obtained from Otsu's thresholding and the volume fraction error compared to the theoretical pore volume fraction.
2 Increment the threshold T_1 by a small amount if the error is positive or decrement it if the error is negative.
3 Apply the revised threshold T_1 on the image and recalculate the pore volume fraction error.
4 Stop if the error is less than required tolerance, else go to step 3.

The algorithm also reduces the increment/decrement step sizes in the case of error signs changing during a step to achieve better accuracy for the pore volume fraction. This step results in a corrected volume fraction for the pore phase based on theoretical values. However, still the Ni volume fraction is under-represented while the YSZ volume fraction is over–represented. This mainly results from some packets of YSZ inside Ni regions and thin layers of YSZ particles formed around the Ni particles (Fig. 1), which was also mentioned in [15]. The next step of the algorithm addresses this problem by performing the sweep-fill operation. The goal of this operation is to identify and fill the YSZ packets and thin layers with Ni increasing the Ni content and thereby improving the accuracy of the segmentation.

The operation sweeps the image pixels in four directions (right to left, left to right, top to bottom and bottom to top) and fills pixels with Ni phase subject to some conditions. The algorithm steps are detailed in the following.

1 Detect change from Ni to YSZ in adjacent pixels by comparing the current pixel colour with the previous one.
2 If change is detected, check the colour of ‘jump’ number of subsequent pixels in the row/column including the current pixel.
3 If one or more of them correspond to either pore or Ni, then replace all the jump number of pixels with Ni.
4 Continue the sweep and if change detected go to step 1.
5 After completing the sweep in all four directions, calculate the current Ni volume fraction.
6 Terminate if the change in Ni volume fraction is smaller than a given ‘Del’, else proceed to another round of sweep fill.

The ‘jump’ is an adjustable parameter that can be used to control the thickness of filling in order to achieve best results. At the end of the sweep-fill operation, the volume fractions of the Ni and YSZ are closer to the theoretical values, while the pore volume fraction is nearly unchanged.

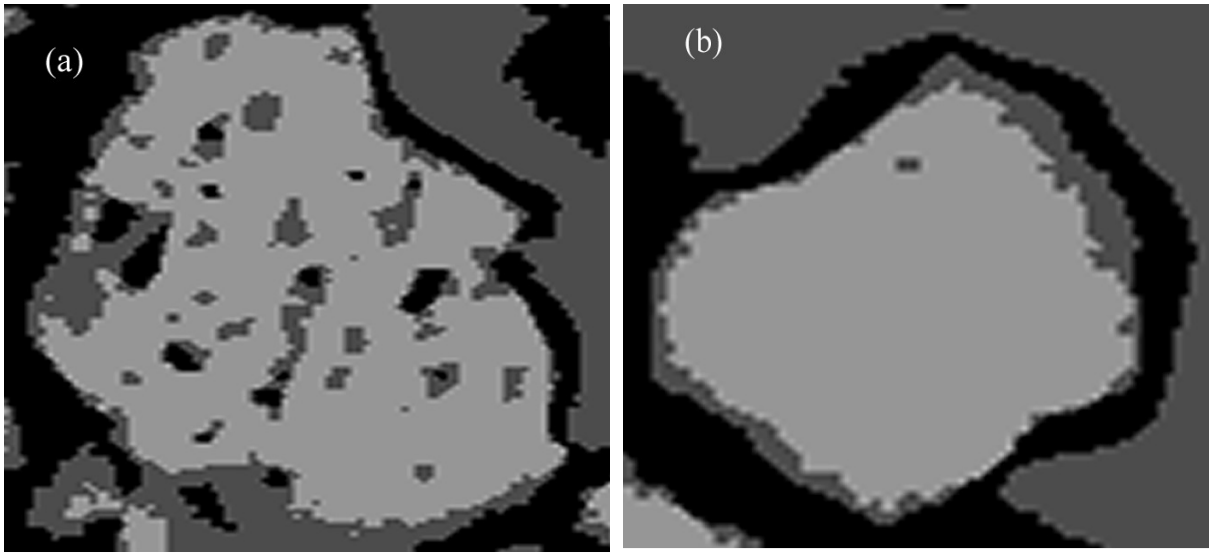

Fig. 1: YSZ packets and thin layers on the image obtained after the auto thresholding operation.

Further image refinement is performed using the morphological operations of erosion and dilation. A disk type structuring element with an adjustable radius ‘r’ is used for performing these operations. The radius of the element is an adjustable parameter. A radius of 1 pixel is generally suitable. This morphological operation has the effect of closing small gaps and smoothing sharp edges. Figures depicting the effect of this algorithm on a sample microstructure are provided in Fig. 2.

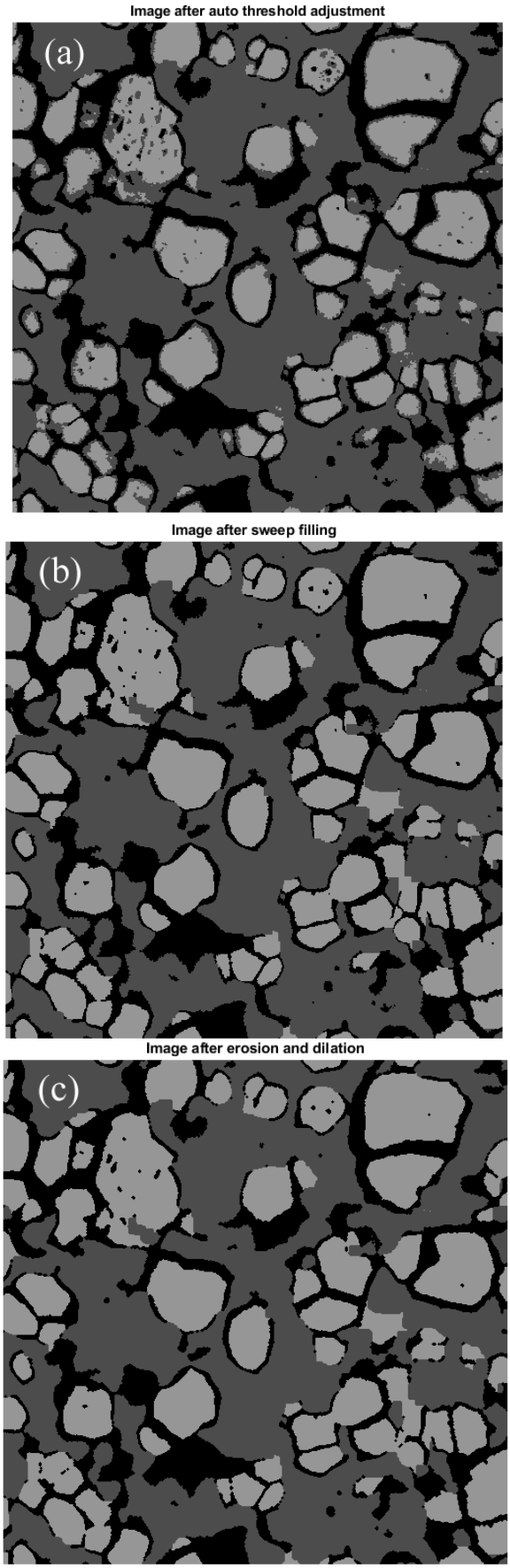

Fig. 2: Anode images after undergoing different steps of the proposed compound algorithm.

3. Properties calculation

The properties of the microstructure including the particle sizes, surface and interface areas, triple phase boundary (TPB) densities and contact angles are extracted from the segmented images. The principles of stereology are exploited in calculating these properties.

Particle sizes

The Ni and YSZ particles sizes are measured using the line intercept method. In this method, a number of random lines are drawn on the image and the intersections of the lines with the particle boundaries are counted.

$$D_i = 1.5\frac{L\psi_i}{N_i} \quad (1)$$

Where, L is the total length of the lines, V_i is the volume fraction of the phase '*i*', and N_i is the number of grains of phase '*i*' crossed by the line. The factor 1.5 is used to obtain the equivalent spherical diameter of the grain [6].

Binary images of the Ni, YSZ and the pore phases are first derived from the segmented images, on which the line intercept method is applied. The binary image of a phase will show the concerned phase in white while the pixels representing the other two phases are shown in black. In this work, the lines that are used in calculating the particle sizes start at random points along an edge and will have randomly generated slopes. The lines end at their intersection points with any of the other three image edges. Thus, the lengths of the lines are also random. Such random lines are generated starting from all the four edges of the image for uniformly covering the image area. The particle size calculations reported in this work are obtained by using 100 lines starting from each edge of the image and thus considers totally 400 lines in the image. Calculation of the particle sizes using the line intercept method involves image binarisation. The binary image of a phase will show the concerned phase in white while the pixels representing the other two phases are shown in black as presented in Fig. 3a, 3b and 3c. An example for the lines generated for size calculation is shown in Fig. 3d.

Many methods are used for deriving particle sizes other than the line intercept method. Feret diameter is a concept akin to measuring the particles with a calliper. The distance between tangents to the particle profile at any predefined direction is the Feret diameter. Another method is the equivalent diameter that is the diameter of a circle equivalent in area to the particle. Yet another method for particle size measurement is the local thickness approach used in ImageJ. Particle size is measured as structure thickness which is also known as local thickness [7] measured at any given point in the structure as diameter of the largest circle that contains that point and fills completely inside the structure. As a means of additional validation for the line intercept particle size measurement method, the size of the Ni particles were also measured using the preceding three methods and the comparison is shown in Fig. 4a. The line intercept method is seen to provide a measurement somewhere between the values provided by other methods. Provided that the accuracy of the line intercept method can be improved by increasing the number of lines, this method is recommended in this work. Similar comparison of the YSZ particle size with the local thickness method is presented in Fig. 4b. The equivalent diameter or Feret diameter cannot be used for calculating YSZ particle size due to its continuous morphology.

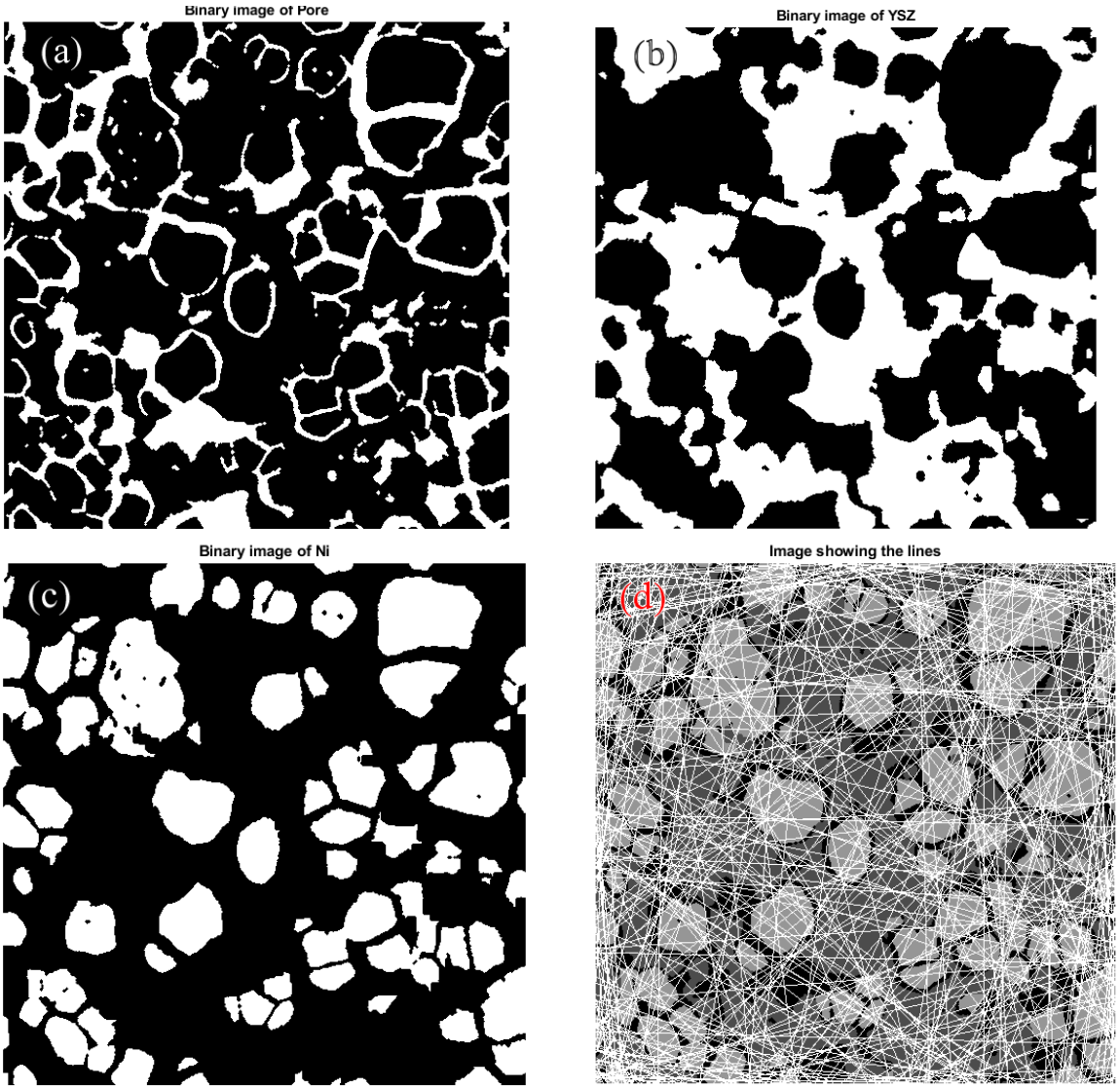

Fig. 3: Binary images of the phases and lines generated for calculating particle sizes.

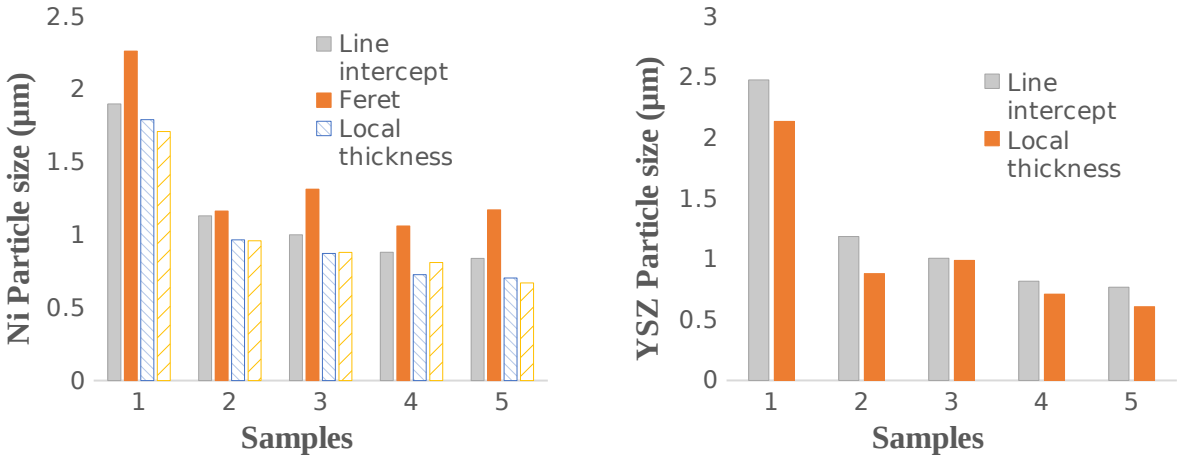

Fig. 4: Comparison of different methods for particle size determination.

Surface and interface areas

The surface areas of the individual phases are calculated based on the following stereological relation [24].

$$S_i = \frac{4}{\pi} L_i \tag{2}$$

where L_i is the perimeter of the phase per unit area.

The surface area of a phase consists of interface areas with other phases.

$$S_{Ni} = S_{Ni,YSZ} + S_{Ni,pore} \tag{3}$$

$$S_{YSZ} = S_{Ni,YSZ} + S_{YSZ,pore} \tag{4}$$

$$S_{pore} = S_{Ni,pore} + S_{YSZ,pore} \tag{5}$$

Since the surface area of a phase can be considered as a sum of interface areas with the two other phases as given in Eqs. 3-5, we can obtain the three interface areas as follows.

$$S_{Ni,YSZ} = \left(S_{Ni} + S_{YSZ} - S_{pore} \right) / 2 \tag{6}$$

$$S_{Ni,pore} = \left(S_{Ni} - S_{YSZ} + S_{pore} \right) / 2 \tag{7}$$

$$S_{YSZ,pore} = \left(S_{YSZ} + S_{pore} - S_{Ni} \right) / 2 \tag{8}$$

Figure 5 shows the perimeters of the phases extracted from the segmented images.

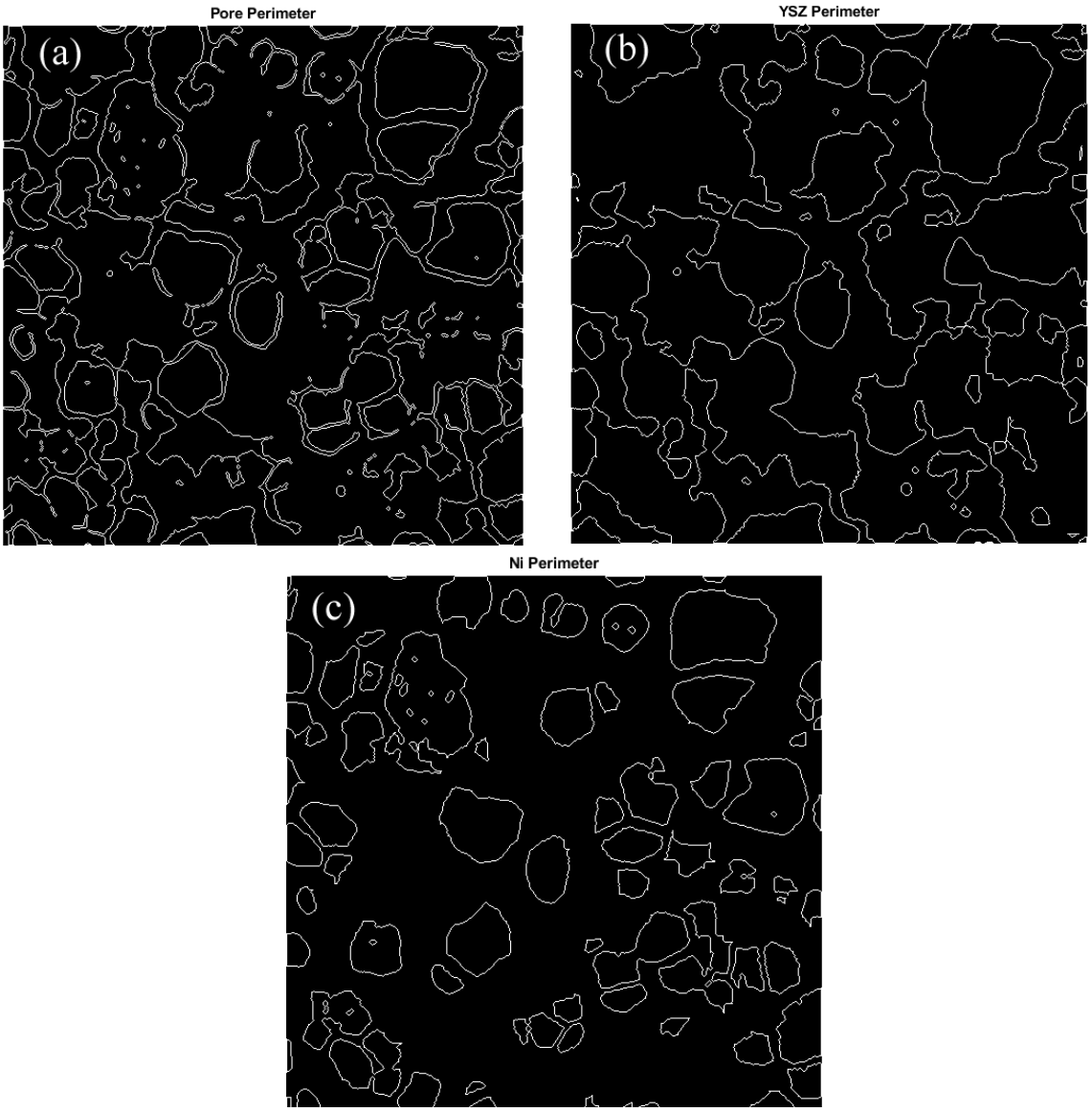

Fig. 5: The phase perimeters generated for calculating the surface and the interface areas.

Triple phase boundary densities

Triple phase boundaries are the regions where all the three phases are meet. These are the regions that actually support the electrochemical reactions and therefore very important for evaluating cell performance. The TPB length per unit volume is evaluated using the following stereological relation [5].

$$\lambda_{TPB} = 2P_A \tag{9}$$

where, λ_{TPB} is TPB length per unit volume and, P_A are the points of interest per unit area of image. TPB points in the image are identified by scanning the sample image using a 2x2 pixels square structural element and counting the number of such 2x2 squares in the image containing all the three phases. The TPB points identified in a sample anode microstructure is shown in Fig. 6.

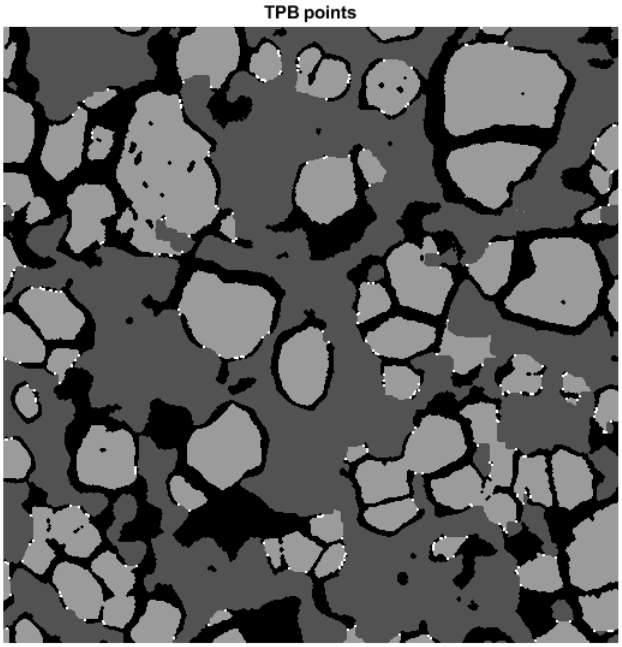

Fig. 6: Image depicting the TPB points identified by the software application The white dots are the 2x2 pixel TPB points.

Contact angles

Contact angles between the phases is a variable that is used in microstructure modelling based on spherical particle assumptions [25-29]. The contact angles as defined in these microstructural models cannot be measured. Another definition of contact angles was provided in [30], where they defined as the angles subtended by the phases around the TPB points and they were derived from three dimensionally reconstructed electrodes. A possible transformation between these two definitions for contact angle was provided in our earlier publication [28]. Here I attempt to derive contact angles from the 2 dimensional images.

Since the contact angles are defined as the angles subtended by the three phases around the TPB points, the algorithm for extracting the contact angles must identify the intersections between the phases around the TPB points (Fig. 7a). The figure shows the intersection points on the second layer around the TPB point. The phase intersection point at the 2x2 domain of the TPB pointis obtained by scanning the domain to detect change in pixel intensities. The mid-point of the two pixels with varying phases is considered as the intersection point and the angle of the line connecting this to the TPB point is constructed for calculating the contact angles. However, more accuracy can be obtained by identifying the intersections at more concentric layers around the TPB point.

For calculation of the contact angles, the TPB point is considered as the middle point in the pixel square and the four pixels immediately around will form the first layer. The layer is scanned starting from the top left pixel and phase intersections are identified. For the first layer shown in Fig. 7a, 12 pixels are scanned and three intersection points are identified as shown as circular spots. The angles subtended by the line joining the spots and the central TPB point are measured as, α_1, α_2 and α_3. They are then converted into the actual angles subtended between the phases ϕ_1, ϕ_2 and ϕ_3. These angles can vary slightly depending on the layers on which they are measured as illustrated in Fig. 7b. This figure shows the intersection points on four layers around the TPB point and the corresponding slopes of the lines connecting them with the TPB point.

For better accuracy, the average of the four angles resulting from scanning the four concentric layers surrounding the TPB point is considered for contact angle calculation. The average angle of the intersections between the phases are represented by dashed lines in Fig. 7b. Sometimes, more than three phase intersections are possible around the TPB points due to reasons like the presence of tiny particles. Only the TPB points that result in three interfaces in the surrounding pixels are

considered for angle calculation. The angles of each phase is averaged over all the TPB points to obtain the average contact angle for the phase in the image sample. It can be seen that the distribution of the pore, Ni and YSZ angles roughly follow a normal distribution as presented in Fig. 8.

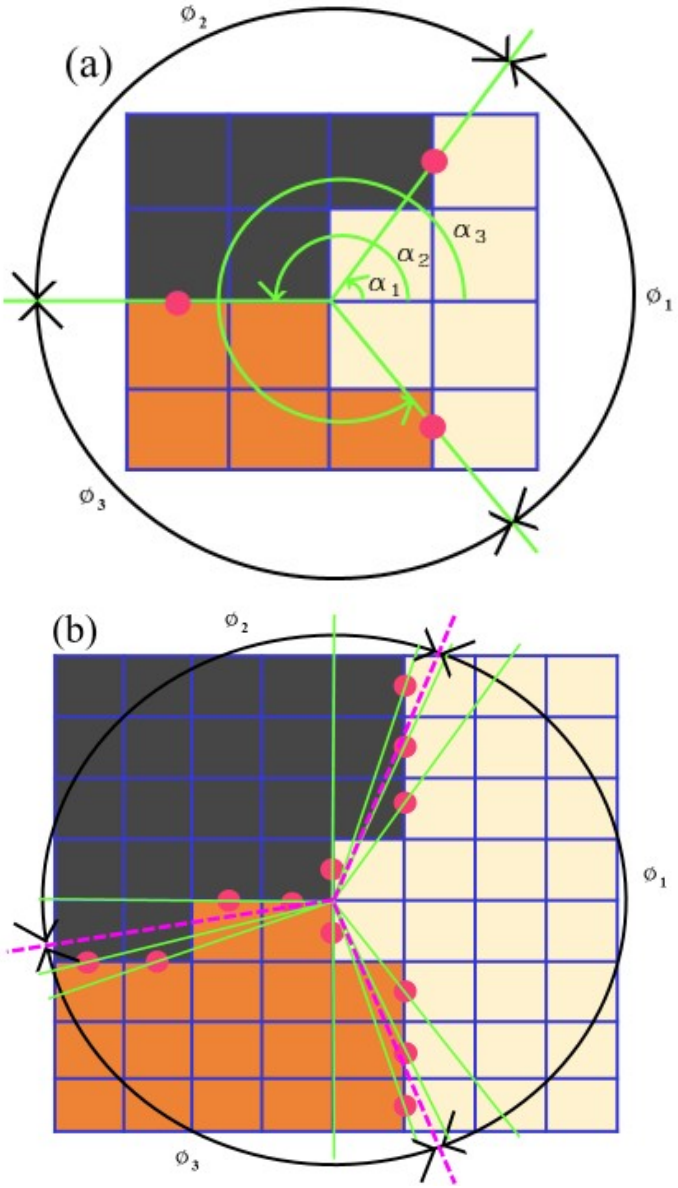

Fig. 7: Illustration of the contact angle calculation.

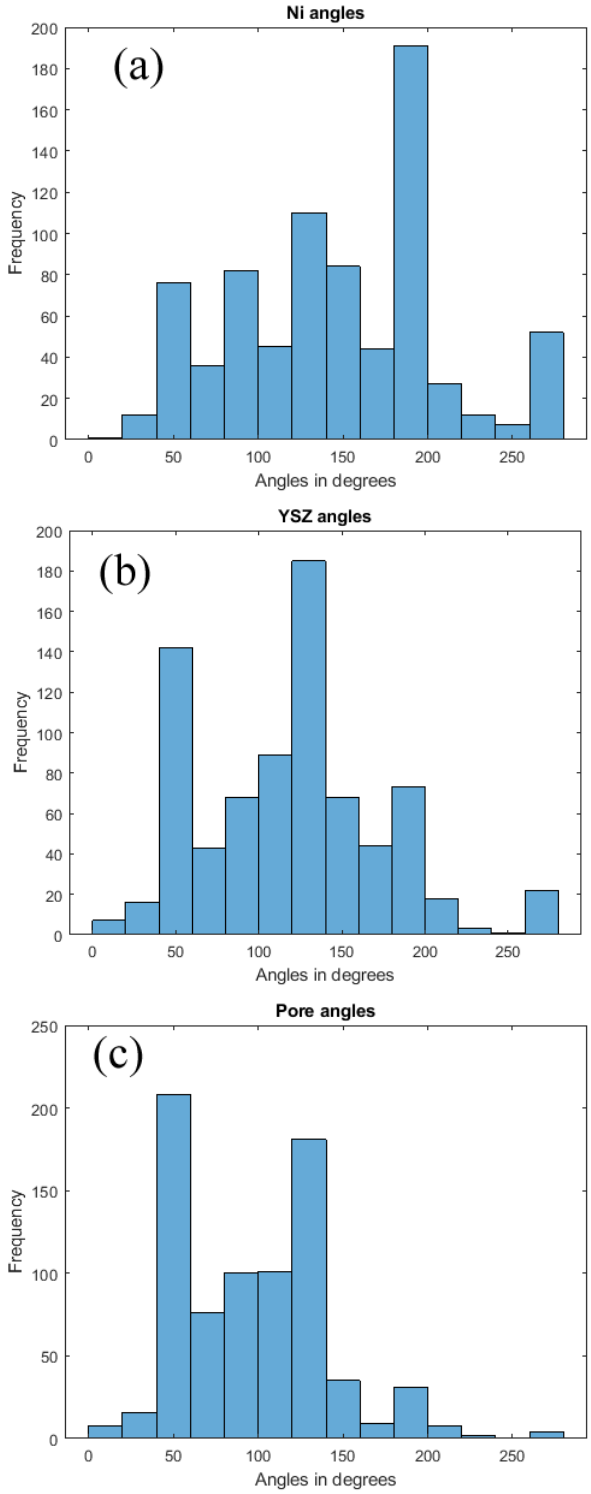

Fig. 8: The contact angle distributions for the phases reported by the application.

4. Matlab application for SOFC image processing

A graphical user interface (GUI) based application has been created in Matlab for SOFC electrode image processing and property calculation based on the algorithms presented in this article. A screenshot of the image processing step 1 tab of the application is presented in Fig. 9. We can load the image file to be analysed into the application by opening and selecting the desired file by clicking the ‘Load image’ button. The histogram for that image can be generated by clicking the ‘Plot Image Histogram’ button. In the ‘Step 1’ image processing tab, the theoretical pore volume

fraction and the error tolerance are input to perform the Otsu's thresholding and adjustment of the threshold T_1. The calculated thresholds are automatically updated on the sliders and the resulting image is displayed on the image display window on the right by clicking the 'Auto Adjust Thresholds' button. In addition, the image is also displayed on a separate window for saving. Further manual adjustment of the thresholds, if desired, can be performed by dragging the sliders and clicking the 'Update thresholds' button. This action updates the thresholds, displays images on image window and also opens image in separate window for saving. The volume fractions in the image after each operation are also calculated and all data are automatically saved to a data file. The tab IP step2 opens options for performing the sweep filling, the erosion and dilation steps. The parameters of 'jump', 'Del' and the radius 'r' for the structuring element are the inputs. The generated images are displayed on the image window on the right and on separate figures for saving.

The property calculation tab opens options to calculate particle sizes, surface areas, TPB densities and contact angles. The input parameters for this are the image dimensions in μm, kn and P. kn and P are the parameters used while performing the line intercept method for particle size calculation. The parameter 'kn' is the number of random lines starting from each edge of the image used in particle size calculation and the total number of lines would therefore be 4 times kn. An operation to remove particles less than P pixels is performed so that the particle counting is not affected by these. Typical value used for P in this work is 8. All the images in this article are generated by the application.

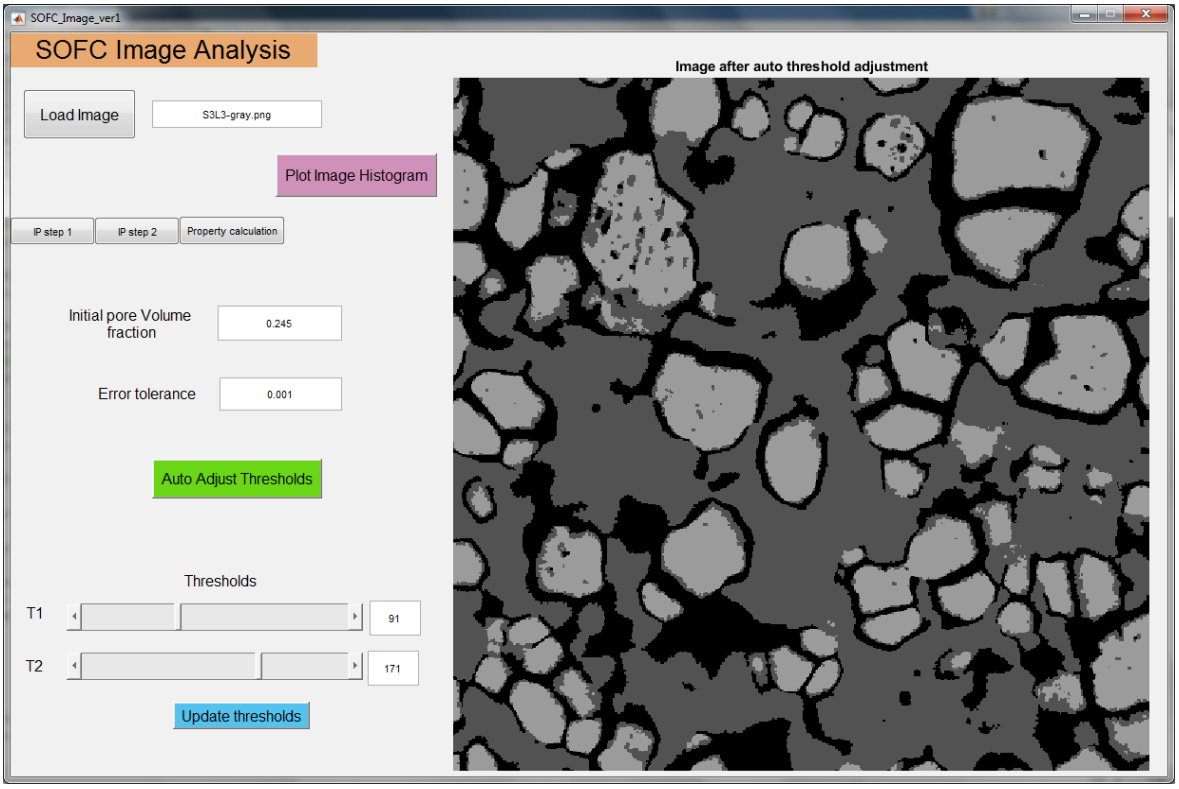

Fig. 9: A screenshot of the Matlab application developed for SOFC image processing.

5. Conclusions

Extracting the microstructural properties of SOFC electrodes from images is required for optimising and tailoring the microstructure to obtain best performance. Addressing the lack of established methods for SOFC electrode image segmentation, the article proposes a compound algorithm comprising of thresholding and other morphological operations. The algorithm minimises the volume fraction errors and involves only a few adjustable parameters to achieve successful segmentation. Algorithms for calculating the microstructural properties from the segmented images are presented. In particular, the algorithm for measurement of contact angles from 2D images is

presented. All these methods are implemented on Matlab as a graphical user interface based application useful for SOFC image analysis. The application code is available as an open source software with the Apache License 2.0 license at the following Github URL: https://github.com/Devetree/SOFC-IMG

Nomenclature:

θ	Contact angle between spherical particles (degrees)
Z	Overall average coordination number of all particles
n	Number of particles per unit volume
r	Radius of particles (μm)
ε	Electrode porosity
ψ	Volume fraction
λ	Triple phase boundary density (μm^{-2})
ϕ	Angle subtended by the phase about the TPB point (degrees)
$Z_{i,j}$	Average number of *i* particles in contact with an *j* particle
ξ	Number fraction
$\min(r_i, r_j)$	Minimum of r_i and r_j
S	Surface area per unit volume
C	Contact area per unit volume
L	Perimeter of a phase per unit area

References

[1] Simwonis D, Tietz F, Stöver D. Nickel coarsening in annealed Ni/8YSZ anode substrates for solid oxide fuel cells. Solid State Ionics. 2000;132:241-51.

[2] Lee KR, Choi SH, Kim J, Lee HW, Lee JH. Viable image analyzing method to characterize the microstructure and the properties of the Ni/YSZ cermet anode of SOFC. Journal of Power Sources. 2005;140:226-34.

[3] Lee J-H, Moon H, Lee H-W, Kim J, Kim J-D, Yoon K-H. Quantitative analysis of microstructure and its related electrical property of SOFC anode, Ni–YSZ cermet. Solid State Ionics. 2002;148:15-26.

[4] Thyden K. Microstructural characterization of SOFC Ni–YSZ anode composites by low-voltage scanning electron microscopy. Solid State Ionics. 2008;178:1984-9.

[5] Faes A, Hessler-Wyser A, Presvytes D, Vayenas CG, Van herle J. Nickelâ Zirconia Anode Degradation and Triple Phase Boundary Quantification from Microstructural Analysis. Fuel Cells. 2009;9:841-51.

[6] Monachon C, Hessler-Wyser A, Faes A, Faes A, Van Herle J, Tagliaferri E. Rapid Preparation and SEM Microstructural Characterization of Nickel-Yttria-Stabilized Zirconia Cermets. Journal of the American Ceramic Society. 2008;91:3405-7.

[7] Lanzini A, Leone P, Asinari P. Microstructural characterization of solid oxide fuel cell electrodes by image analysis technique. Journal of Power Sources. 2009;194:408-22.

[8] Vivet N, Chupin S, Estrade E, Piquero T, Pommier PL, Rochais D, et al. 3D Microstructural characterization of a solid oxide fuel cell anode reconstructed by focused ion beam tomography. Journal of Power Sources. 2011;196:7541-9.
[9] Joos J, Carraro T, Weber A, Ivers-Tiffée E. Reconstruction of porous electrodes by FIB/SEM for detailed microstructure modeling. Journal of Power Sources. 2011;196:7302-7.
[10] Brus G, Iwai H, Otani Y, Saito M, Yoshida H, Szmyd JS. Local Evolution of Triple Phase Boundary in Solid Oxide Fuel Cell Stack After Long-term Operation. Fuel Cells. 2015;15:545-8.
[11] Kwok K, Jørgensen PS, Frandsen HL, Wakai F. Computation of Effective Steady-State Creep of Porous Ni-YSZ Composites with Reconstructed Microstructures. Journal of the American Ceramic Society. 2015;98:2873-80.
[12] Mújica-Vargas D, Gallegos-Funes FJ, Rosales-Silva AJ. A fuzzy clustering algorithm with spatial robust estimation constraint for noisy color image segmentation. Pattern Recognition Letters. 2013;34:400-13.
[13] Fu X, Xiang Y, Chen L, Xu X, Li X. A Novel Ni/YSZ Anode Image Segmentation Method for Solid Oxide Fuel Cell Electrodes Microstructure. Fuel Cells. 2016;16:810-21.
[14] Gunda NSK, Choi H-W, Berson A, Kenney B, Karan K, Pharoah JG, et al. Focused ion beam-scanning electron microscopy on solid-oxide fuel-cell electrode: Image analysis and computing effective transport properties. Journal of Power Sources. 2011;196:3592-603.
[15] Joos J, Ender M, Rotscholl I, Menzler NH, Ivers-Tiffée E. Quantification of double-layer Ni/YSZ fuel cell anodes from focused ion beam tomography data. Journal of Power Sources. 2014;246:819-30.
[16] Ni C, Cassidy M, Irvine JTS. Image analysis of the porous yttria-stabilized zirconia (YSZ) structure for a lanthanum ferrite-impregnated solid oxide fuel cell (SOFC) electrode. Journal of the European Ceramic Society. 2018;38:5463-70.
[17] Russ JC, Neal FB. The Image Processing Handbook: CRC Press 2017.
[18] Yang X, Fu X, Li X. Adaptive Clustering SOFC Image Segmentation Based on Particle Swarm Optimization. Journal of Physics: Conference Series. 2019;1229:012020.
[19] Wilson JR, Cronin JS, Barnett SA. Linking the microstructure, performance and durability of Ni-yttria-stabilized zirconia solid oxide fuel cell anodes using three-dimensional focused ion beam–scanning electron microscopy imaging. Scripta Materialia. 2011;65:67-72.
[20] Vivet N, Chupin S, Estrade E, Richard A, Bonnamy S, Rochais D, et al. Effect of Ni content in SOFC Ni-YSZ cermets: A three-dimensional study by FIB-SEM tomography. Journal of Power Sources. 2011;196:9989-97.
[21] Shearing PR, Gelb J, Yi J, Lee WK, Drakopolous M, Brandon NP. Analysis of triple phase contact in Ni–YSZ microstructures using non-destructive X-ray tomography with synchrotron radiation. Electrochemistry Communications. 2010;12:1021-4.
[22] Lee K, Choi S, Kim J, Lee H, Lee J. Viable image analyzing method to characterize the microstructure and the properties of the Ni/YSZ cermet anode of SOFC. Journal of Power Sources. 2005;140:226-34.
[23] Holzer L, Münch B, Iwanschitz B, Cantoni M, Hocker T, Graule T. Quantitative relationships between composition, particle size, triple phase boundary length and surface area in nickel-cermet anodes for Solid Oxide Fuel Cells. Journal of Power Sources. 2011;196:7076-89.
[24] EE U. Quantitative Stereology for Microstructural Analysis. Boston, MA: Springer US; 1973.
[25] Chen D, He H, Zhang D, Wang H, Ni M. Percolation Theory in Solid Oxide Fuel Cell Composite Electrodes with a Mixed Electronic and Ionic Conductor. Energies. 2013;6:1632-56.
[26] Chen D, Lin Z, Zhu H, Kee RJ. Percolation theory to predict effective properties of solid oxide fuel-cell composite electrodes. Journal of Power Sources. 2009;191:240-52.
[27] Chen D, Zhang Q, Lu L, Periasamy V, Tade MO, Shao Z. Multi scale and physics models for intermediate and low temperatures H + -solid oxide fuel cells with H + /e − /O 2− mixed conducting properties: Part A, generalized percolation theory for LSCF-SDC-BZCY 3-component cathodes. Journal of Power Sources. 2016;303:305-16.

[28] Vijay P, Tadé MO, Shao Z. Model based evaluation of the electrochemical reaction sites in solid oxide fuel cell electrodes. International Journal of Hydrogen Energy. 2019;44:8439-59.
[29] Vijay P, Tadé MO, Shao Z, Ni M. Modelling the triple phase boundary length in infiltrated SOFC electrodes. International Journal of Hydrogen Energy. 2017;42:28836-51.
[30] Sun X, Hasegawa Y, Kohno H, Jiao Z, Hayakawa K, Okita K, et al. Calculation of contact angles at triple phase boundary in solid oxide fuel cell anode using the level set method. Materials Characterization. 2014;96:100-7.